NASA TT F-10,250

NASA TT F-10,250

STATE OF DEVELOPMENT OF THE GIESSEN ION ENGINE

H. Löb

Translation of "Entwicklungsstand des Giessener Ionentriebwerkes". Paper presented at the Symposium on Electrical Space Motion, Sonnenberg, West Germany, Feb. 24, 1966. Deutsche Gesellschaft für Raketentechnik und Raumfahrtforschung, 13 pp.

NATIONAL AERONAUTICS AND SPACE ADMINISTRATION
WASHINGTON AUGUST 1966

NASA TT F-10,250

STATE OF DEVELOPMENT OF THE GIESSEN ION ENGINE **/1

H. Löb*

Results of a study to improve the absolute and specific power outputs of an electrostatic test engine being developed at the University of Giessen. The results cited mainly concern the ionizer, since this is said to be the part of the engine which differs most from American models. The ionizer in this case is a high-frequency ion source distinguished by the fact that it allows mercury to be used as the propellant, creates only singly charged ions, is simple to build, and is lightweight and long-lasting. It is shown that such a high-frequency ion source can be developed by increasing the discharge intensity with the aid of a weak, constant magnetic field and by improving the process of ion extraction. author

1. Synopsis

By the end of 1965, the investigations at the First Physical Institute Giessen on the laboratory model of an electrostatic power plant were successfully concluded.

After preliminary work over a period of four years, the tests were started in April 1964.

---

* Physical Institute of the University Giessen.

** Numbers in the margin indicate pagination in the original foreign text.

The first results were discussed at the Combined Annual Meeting of the WGLR and the DGRR* on September 14–18, 1964 in Berlin (Bibl.1). Over the following 15 months, the absolute and specific performance of the test engine were greatly increased by optimizing the geometry and the operating parameters, as shown in the comparison below. The size of the engine itself was not changed.

	September 1964	December 1965
Ion current J_{ii}	8 ma	39 ma
Thrust $S = J_{ii} \cdot m_i/e_i \cdot v_T$	0.2 pond**	1 pond
Jet power $L = S \cdot v_T/2$	120 w	585 w
Power loss L_v	40 w	85 w
Total power $L + L_v$	160 w	670 w
Electric efficiency $\eta_e = L(L + L_v)$	75%	87%
Mass efficiency $\eta_m = J_{ii}/(J_{ii} + e_i J_O)$	90%	95%
Total efficiency $\eta_{tot} = \eta_e \cdot \eta_m$	67.5%	83%

(Here, m_i = ion mass, e_i = ion charge, v_T = rate of propellant flow, J_O = = neutral gas stream.)

The investigations on engine optimizing were used by the graduate physicist J.Freisinger in his thesis.

2. Current Projects

At present, the experimental engine is being converted to practical operating conditions. The work comprises five points:

---

* WGLR = Wissenschaftliche Gesellschaft für Luft- und Raumfahrt (Scientific Association for Aeronautics and Space); DGGR = Deutsche Gesellschaft für Raketentechnik und Raumfahrtforschung (German Society for Rocket Technique and Space Research).

** pond = weight of mass unit = 980.665 dynes = pound.

1) The engine mass will be minimized; operational reliability and ruggedness must not be impaired by this. The engine mass is estimated as 1 kg.

2) The engine will be simplified as far as possible. Flexibility and exchangeability of individual structural parts, in contrast to the experimental engine, are not required in the full-scale model. /2

3) The engine will be designed with sufficient ruggedness to withstand accelerations up to 15 g_0, strong vibrations, etc. for short periods of time without damage. The engine must operate reliably also in the weightless state. Investigations in this direction are in preparation.

4) The engine will be subjected to long-time tests. During these endurance tests, the operational data will be automatically adjusted to optimum values. The engine must be easy to cut in and out repeatedly, and the thrust must be variable within wide limits at a low control power.

5) The neutralizer must be properly adjusted and the jet neutralization accurately measured. For this, a space test would be desirable.

In accordance with this conversion, the high-frequency transmitter of the ion source is being transistorized at present and equipped with a spiral tank circuit. The mercury boiler is so designed that the propellant is evaporated by the waste heat of the transmitter or of the discharge. This eliminates the necessity of separate evaporator heating.

The projects are managed by M.Schäfer and F.Trojan. The work is still in progress so that no final statements can be made at present.

Below, we will discuss the investigations performed over the period of

September 1964 to December 1965, which resulted in the above-mentioned improvement in engine performance. As known, an ion engine consists of a propellant tank, an evaporator, an ionizer, an accelerator, and a neutralizer. Our investigations centered primarily on the ionizer, especially since our engine differs from the American design in this particular point.

As ionizer, we are using a high-frequency ion source. This device permits the use of mercury as propellant, generates only singly charged ions, is simple in design, light in weight, and has a long service life. Our main problem was to develop a HF ion source of this type, of optimum efficiency. This goal was reached by increasing the discharge intensity (Sect.4) and by improving the extraction (Sect.6). In order to interpret the measurements, we will first briefly outline the mechanism of HF discharge (Sect.3) and the theory of extraction (Sect.5).

3. Mechanism of HF Discharge

The propellant is fed from the evaporator to the ion source. This source consists of a discharge vessel, a high-frequency transmitter, and an extraction device. The extracted fuel ions travel from here to the accelerator and /3
neutralizer.

The discharge vessel has a cylindrical shape, consisting of insulating material, and is in contact with the moving coil of the transmitter.

The transmitter coil induces a HF electric eddy field in the discharge vessel, having a field strength of

$$|\mathfrak{E}_{ind}| = \frac{1}{2} \mu_0 \frac{n}{\ell} r J_{HF} \omega \sin \omega t = |\mathfrak{E}_0| \sin \omega t \qquad (1)$$

where μ_0 = induction constant; n = number of turns; ℓ = coil length; r = axial spacing; J_{HF} = current amplitude of the transmitter coil; ω = angular velocity of the transmitter; t = time.

$\mathfrak{E}_{ind}$ depends on the transmitter power, over J_{HF}.

If electrons are present in the discharge vessels, they will be accelerated in the electric eddy field. Their energy increment during one-half HF period τ is computed as

$$\Delta E_e = 2 \frac{e}{\omega} |\mathfrak{E}_0| \cdot \left(\frac{e|\mathfrak{E}_0|}{m_e \omega} + v_e \right) \qquad (2)$$

where e = elementary charge; m_e = electron mass; v_e = initial velocity of the electrons.

In our case (n/ℓ = 0.67/cm, r = 4.3 cm, J_{HF} = 2 amp, and $\omega = 1.1 \times 10^8$/sec), the amplitude of the induced electric field strength $|\mathfrak{E}_0|$ will be 4.1 v/cm. From this, the energy increment of an electron at rest (v_e = 0) during one half-period can be calculated as ΔE_e = 2.15 ev. Thus, this electron is unable to ionize a mercury atom (with an ionization potential of E_i = 10.4 ev). In the next negative HF half-period, it would again be decelerated.

However, if the electron, after termination of the acceleration phase, undergoes an elastic collision with a neutral gas atom, during which its direction of motion changes by 180^0, it will be further accelerated in the subsequent half-period. Now the electron starts with an initial energy of 2.15 ev or an initial velocity of $v_e = 8.7 \times 10^7$ cm/sec, with the energy increment being 6.45 ev and the terminal energy 8.6 ev. After another reversal of direction, the electron will be able to ionize.

In general, the elastic collisions will not always occur at the optimum instant of time or with exactly a 180^0 change in direction, so that the ionizing electrons, in the statistical mean, must execute more than two collisions before they can accumulate the required energy.

By a suitable selection of the gas pressure p, this process can be influenced in a favorable sense: If the mean free time of flight of the electrons is equal to a HF half-period τ, an especially large number of electrons will undergo reversal collisions at the correct instant. From τ and the mean electron velocity $\bar{v}_e$, the optimum mean free path of the electrons can be /4
calculated:

$$\lambda_e = \bar{v}_e \cdot \tau = 4\sqrt{2}\,\lambda_0, \quad \lambda_0 = \frac{kT_0}{\sqrt{2}\,\pi d_0^2 p} \tag{3}$$

where λ_0 is the mean free path, T_0 the temperature, d_0 the diameter of the neutral gas particles, and k the Boltzmann constant. Setting

$$\bar{v}_e = \sqrt{\frac{8kT_e}{\pi m_e}} = 6.15 \times 10^5 \text{ cm/sec} \cdot \sqrt{T_e/{}^\circ\mathrm{K}} \tag{4}$$

we obtain the optimum gas pressure

$$p_{opt} = \frac{C_1}{\sqrt{T_e} \cdot \tau} \quad C_1 = \sqrt{\frac{2km_e}{\pi}} \cdot \frac{T_0}{d_0^2} = 1.7 \times 10^{-8} \text{ torr sec} \sqrt{{}^\circ\mathrm{K}}. \tag{5}$$

In our case ($T_e = 2.6 \times 10^4$ °K, $\tau = 2.9 \times 10^{-8}$ sec, $T_0 = 350$°K), the optimum gas pressure p_{opt} is obtained as 3.7×10^{-3} torr. If the pressure is higher, the electron temperature will drop; if p is decreased, the discharge will be extinguished.

The gas or the vapor in the ion source is ionized by collisions of electrons which have absorbed their energy from the high-frequency field in the described manner*.

This leads to the formation of a self-sustaining electrodeless high-

---

* The ignition of the HF discharge does not take place through the induced eddy field $\mathfrak{E}_{ind}$ but over the capacitatively coupled HF field $\mathfrak{E}_{cap}$, generated between the individual coil windings and having a higher field strength. After ignition, the capacitative field is shielded by the plasma, and the eddy field takes over maintenance of the discharge in the described manner (Bibl.2).

frequency gas discharge. In the discharge vessel, a luminescent quasi-neutral nonisothermal plasma is created. The ion density n_i and the electron density n_e are statistically equal. In our case (100 w transmitter power) they are $5 \times \times 10^{10}/cm^3$, being by about three orders of magnitude below the neutral gas density of $n_0 = 10^{14}/cm^3$. The electron temperature T_e is 2.6×10^4 °K, while the ion temperature T_i is only slightly above the neutral gas temperature of $T_0 = 350$°K. The reason for this lies in the low energy absorption and the high elastic energy losses of the ions, both due to their large mass.

The balance equation of the plasma states that, at equilibrium, the number of charge carriers newly formed by ionization, is equal to the carrier depletion. The number of ionization events by fast electrons with Maxwellian velocity distribution, in mercury per unit time dt, is as follows:

/5

$$\frac{dN_i}{dt} = C_2 \frac{n_i}{e_i} p V_v \exp(-C_3) \cdot \frac{0.5 + 1/C_3}{\sqrt{C_3}}$$

$$C_2 = 4\sqrt{\frac{2}{\pi}} \cdot a \cdot \frac{E_i^{3/2}}{\sqrt{m_e}} = 6.73 \times 10^{-10} \frac{\text{amp}}{\text{torr}},\ C_3 = \frac{E_i}{kT_e} \qquad (6)$$

where V_v is the vessel volume and a the constant of differential ionization. In our case ($V_v = 500$ cm^3, $a = 0.93$/cm · v · torr), we have for $e_i \cdot dN_i/dt = = 200$ ma.

Unintentional charge carrier losses occur by recombination as well as by intentional ion extraction from the discharge plasma. The frequency of volume recombinations is low. Most recombination events take place along the vessel wall. The two charge carrier species reach the wall due to the radially directed ambipolar diffusion. A negative space charge layer at the vessel wall promotes removal of the ions and decelerates the more mobile electrons, so that equally many ions and electrons will reach the wall.

The ambipolarly removed ion current on the wall is approximately

$$J_{i\,amb} = C_4 \cdot n_i \cdot b_i \cdot kT_e \cdot F_w, \quad C_4(R) = \frac{dI_0(2.4\ r/R)}{dr} = \frac{1.25}{R} \qquad (7)$$

where R is the radius of the discharge vessel, b_i the ion motility, F_w the wall area, and I_0 a Bessel function of the zeroth order. For R = 4.3 cm, b_i = = 1.1×10^5 cm^2/v-sec, and F_w = 290 cm^2, a value of $J_{i\,amb}$ of 160 ma will be obtained. The extracted ion current J_i is 40 ma (see below).

The ion balance equation is satisfied:

$$e_i \frac{dN_i}{dt} = J_{i\,amb} + J_i, \quad 200\ \text{ma} = 160\ \text{ma} + 40\ \text{ma}. \qquad (8)$$

The number of charge carriers, according to eq.(6), is proportional to the vessel volume V_v whereas the ambipolar losses depend on the wall area F_w [eq.(7)]. Consequently, the discharge vessel must be so dimensioned that V_v/F_w is as large as possible. This requirement is satisfied for cylindrical vessels provided that the diameter is equal to the height. Our measurements confirmed this statement. At fixed diameter, we varied the height within wide limits.

In addition, theoretical considerations permit the conclusion that, at similar enlargement of the engine, $e_i \frac{dN_i}{dt} / J_{i\,amb}$ will increase, leading to an increase in efficiency. American investigations - although with Kaufman sources - confirm this finding (Bibl.3).

4. Influence of a Weak Constant Magnetic Field

It is known that a weak stationary magnetic field improves the power consumption of the plasma in a resonance-like manner (Bibl.4). We also made /6
use of these effects.

Figure 1 shows the ion current J_i^* as a function of the magnetic field strength. The ion current, for H = 0, is standardized to 1. The field H is measured on the axis of the ion source. In general, for producing the magnetic field H, one or several small permanent magnets were used, mounted to the outside of the discharge vessel. The magnetic field was perpendicular to the vessel axis (curve H_P).

The curve $J_i^*(Hp)$ shows a resonance-like rise and a maximum at 10 oersteds. In the optimal case, the ion current was nine times higher than without magneton. The effect, in the case of fixed H, was largely independent of the number, arrangement, and polarity of the permanent magnets. To determine the influence of the field inhomogeneity, the permanent magnets were replaced by Helmholtz coils (curve H_H). This did not change the optimal magnetic field strength and the maximum ion current amplification. A difference between the H_P and H_H curves was detected only at low H values.

Finally, we investigated the influence of an axial magnetic field, again using Helmholtz coils (curve H_{II}). We found two maxima, in which case the improvement factor was lower overall than in a vertical field arrangement.

In practical application, only permanent magnets are in question for generating the magnetic field because of energy reasons, specifically since the Helmholtz coils yielded no additional improvement.

The magnetic effect strongly depends on the operating parameters of discharge, on the transmitter power L_{tr}, and on the gas pressure p. This effect is especially manifest at low powers and low pressures, and was not observed at all at pressures above 10^{-2} torr. The greatest current amplification J_i^*, measured by us, was 34.

Figure 2 shows the influence of the transmitter power L_{tr} on the magnetic effect. Here, the ion current with and without 10-oe magnets $J_i(10\text{ oe})$ or $J_i(0)$, the standardized current $J_i^* = J_i(10\text{ oe})/J_i(0)$, measured at equal transmitter power, and the corresponding electric efficiencies $\eta_e(10\text{ oe})$ resp. $\eta_e(0)$

are plotted as a function of L_{tr}. The curve J_i(10 oe) is shifted with respect to the $J_i(0)$ curve by 20 w toward lower powers. This means that the permanent magnet saves 20 w transmitter power. It is obvious that this shift is of importance especially at low L_{tr} values, as is expressed also in the $J_i^*(L_{tr})$ curve. Naturally, the savings in energy show also in the electric efficiency. The difference in the two η_e curves is especially great at low transmitter /7 powers. At a power of 80 w, the improvement in electric efficiency is 2.5%.

In addition to the savings in power, the stationary magnetic field yields a further improvement: The discharge pressure can be reduced to less than 10^{-4} torr without extinguishing the discharge. The considerations made in Section 3 on the optimum pressure (3.7×10^{-3} torr) are no longer valid when auxiliary magnets are used. As in the case of transmitter power, a displacement takes place but this time toward lower p-values. A decrease in the pressure p, as indicated in Fig.3, not only means an increase in ion current J_i but also, predominantly because of the decreasing neutral-gas losses J_0, a considerable improvement in the mass efficiency η_m.

The explanation for the magnetic effect is quite complex.

The resonance-like behavior permits the assumption that a cooperation of Lorentz force and high-frequency field, similar to the cyclotron effect, might be involved: The electrons execute spiral rotations about the magnetic field lines, and are accelerated by the induced electric HF field at exactly the right instant. This causes them to gain rapidly in energy. The effect is additive with the accumulation collisions (Sect.3). This concept would explain the 20-w equivalence of the magnet. One could also understand then that the cyclotron process occurs especially at low pressures where no gas-kinetic collisions interfere. This process also facilitates the energy absorption of the electrons from the high-frequency field, raises the electron temperature, and increases the number of ionization events in accordance with eq.(6).

The cyclotron resonance frequency f_c reads

$$f_c = \frac{1}{2\pi} \cdot \frac{e}{m_e} \cdot \mu_0 H = 2.8 \frac{mc}{oe} \cdot H. \qquad (9)$$

From this, the computed value for f_c will be 28 mc for H = 10 oe. Conversely, the transmitter frequency f was only 17.5 mc.

This discrepancy means that the magnetic effect represents not only an interaction of Lorentz force and eddy field (Bibl.4); rather, it can be assumed that the stationary field also decelerates the ambipolar diffusion directed radially outward, by reducing the ion motility b_i [eq.(7)]. As demonstrated by the ion balance equation [eq.(8)], most of the newly formed ions are lost again by recombination at the vessel walls. However, any decrease in $J_{i\,amb}$ would mean an increase in J_i. Since the motility m_i is inversely proportional to the gas pressure, any reduction in this pressure can be compensated by the magnetic field without causing an increase in ambipolar loss or extinction of the discharge.

5. Theory of Ion Extraction /8

The intentional charge carrier extraction from the high-frequency plasma is done over an extraction system which consists of a pin-type anode and of a cathode plate which latter forms the bottom of the vessel. The cathode is provided with a number of (Z) bores through which the ions leave the source and enter the afteracceleration space. The extraction anode absorbs a corresponding number of electrons. The extraction cathode is shielded from the plasma by an insulating plate. This so-called plasma boundary armature is also provided with

Z bores which must coincide exactly with the cathode holes. However, the apertures in the plasma boundary armature are wider than those in the cathode (Fig.4).

An extraction direct voltage U_e is supplied between anode and cathode.

According to the Langmuir probe theory, a positive space charge is built up in front of the cathode. This unipolar Langmuir layer (because of $n_e = 0$) appears as dark space and is separated from the luminescent plasma by a plasma boundary layer of about 1 mm thickness, in which the electron concentration decreases exponentially. The plasma is field-free, quasi-neutral, and has plate potential*. Therefore, the total extraction potential drops between the plasma boundary, acting as a virtual anode, and the cathode.

The modern probe theory (Bibl.7) demonstrates that, between the undisturbed plasma and the plasma boundary, there is a transition layer of disturbed plasma (Fig.4). Because of the shadow effect of the ion-absorbing plasma boundary, the ion density n_i ($4.7 \times 10^{10}/cm^3$) is somewhat less in the transition layer than in the plasma. From the energy of the plasma electrons, the following potential gradient is built up at the transition layer which has a thickness of approximately 1 cm:

$$U = \frac{1}{2} \cdot \frac{kT_e}{e} = 4.4 \times 10^{-4} \frac{v}{{}^{\circ}K} \cdot T_e . \tag{10}$$

In our case, the gradient is 1.1 v. This residual field accelerates the ions so that, on entry into the plasma boundary layer, they have a velocity corresponding to half the electron temperature ($T_i = 13{,}000^{\circ}K$):

$$v_i = kT_e/m_i = 6.5 \times 10^2 \frac{cm}{sec} \cdot T_e \; {}^{\circ}K. \tag{11}$$

---

* Because of the high electron motility, the plasma potential ordinarily is slightly above the anode potential (Bibl.5, 6). In our case, the difference is 3 v. In all, 0.8 ma ions and 40.8 ma electrons flow to the anode.

From this, a value of 1.04×10^5 cm/sec is calculated. /9

The ion current, penetrating into the space-charge region, is obtained from the relation

$$J_i = Ze_i n_i v_i F_p \qquad (12)$$

The area F_p of the plasma boundary follows from

$$F_p = (r_p^2 + h_p^2)$$

(r_p and h_p are taken from Fig.4). In our case ($Z = 55$, $r_p = 0.45$ cm, $h_p =$ $= 0.3$ cm), a value of J_i of 39.6 ma is obtained.

The ion current penetrating into the space-charge region is taken up by the extraction field and accelerated toward the cathode. This causes an ion-optical focusing (Bibl.8). As already indicated by the term, the plasma boundary layer is "anchored" at the plasma boundary armature. The walls of this armature are positively charged. Both plasma boundary and equipotential areas (except for the cathode channel transconductance) exhibit concave curvatures. This leads to a pinch. Behind the cathode, the ion beam diverges again, with an aperture angle of about 20° (Bibl.8). If the focus of the ion immersion objective, representing the space charge field, is located exactly in the cathode channel, an optimally-focused case is involved. The useful ion current J_{ii}, i.e., the current able to be afteraccelerated, has a maximum while the loss ion current J_{ik}, striking the cathode has a minimum, so that the degree of focusing f_i becomes optimum:

$$f_i = \frac{J_{ii}}{J_{ii} + J_{ik}}, \quad J_i = J_{ii} + J_{ik} \qquad (13)$$

where f_i depends on the extraction potential U_e and on the ion current J_i [eq.(12)], i.e., indirectly on the transmitter power. If U_e is too high or if L_{tr} is too low, the plasma boundary will show an excessive curvature, the focal length will become too short, and the pinch will be located in front of the cathode hole which creates a so-called "overfocused" state. The conditions are exactly the opposite for the "underfocused" case.

The ion current in the cathodic extraction zone is space-charge limited. In first approximation*, it then follows that

$$J_i = C_5 \cdot ZF_p \cdot \frac{U_e^{3/2}}{d^2}, \quad C_5 = \frac{4}{9} \cdot \epsilon_0 \cdot \sqrt{\frac{2e_i}{m_i}} = 3.9 \times 10^{-6} \frac{\text{ma}}{\text{v}^{3/2}} \qquad (14)$$

[$d = h_p + \ell_p$; see eq.(4); ϵ_0 = dielectric constant]. For $U_e = 4.3$ kv, d = = 1.2 cm, Z = 55, and $F_p = 0.9$ cm^2, the value of J_i will be 40 ma**.

6. Tests for Improving the Extraction /10

To obtain an optimum ion extraction, the most favorable extraction potential U_e must be adjusted and the most suitable geometry must be defined.

In Fig.5, the theoretical ion current J_{ith} (broken curve), the measured ion currents J_i, J_{ii}, J_{iK}, and the degree of focusing f_i (dotted curve) are plotted as a function of the extraction potential U_e. The theoretical ion current is composed of two curve segments: up to 4.3 kv extraction potential, it appears as space-charge-limited current [eq.(14)] and, above 4.3 kv, as saturation current [eq.(12)]. The curve is comparable to a diode characteristic. The measured ion current J_i usually is somewhat higher than J_{ith}. The deviation is proportional to the loss current J_{iK}. This fact seems to indicate that the difference is produced by secondary electrons which are knocked out of the cathode by the current J_{iK}. The J_{ii} and J_{iK} curves indicate that optimum focusing

* The formula is rigorously valid only for a two-dimensional electrode arrangement.

** It should be remembered that F_p as well as d depend to a certain extent on U_e. The ratio F_p/d^2, and thus also J_i, have a minimum at $h_p = 0.23$ cm.

exists between 5 and 6 kv extraction potential. At $U_e = 5.5$ kv, the value for f_i is 98%. Such a high degree of focusing must be required not only because of the electric efficiency ($J_{iK} \cdot U_e = 5.5$ w power loss) but also for reasons of lifetime (cathode sputtering).

Figure 6, in agreement with the theory, proves that the optimum extraction potential U_{eopt} increases with the transmitter power L_{tr}.

The geometry studies primarily concern the configuration of the extraction system, the degree of coverage, and the dimensions of the holes in the plasma boundary armature and in the cathode.

Of all investigated types of systems (cylindrical or conical bores, disk, diaphragm, or Pierce geometries), the simplest - namely, the cylindrical - was also found the best.

The coverage Ω means the total area of all holes in the plasma boundary anchor $Z \cdot \pi r_P^2$, divided by the base area πR^2 of the discharge vessel:

$$\Omega = Z \left(\frac{r_P}{R}\right)^2 \qquad (15)$$

To extract as high an ion current as possible, the coverage Ω should be large without, however, leading to an overlap of adjacent transition layers. Measurements showed that the ion current - at otherwise equal conditions - increases linearly with Ω up to $\Omega = 60\%$. A further increase in Ω was impossible for manufacturing reasons (land between two bores, 1 mm).

Detailed comparative tests showed that, on varying r_P/ℓ_P, the ion current, thrust, and efficiencies - at constant Ω - show a maximum, if r_P/ℓ_P is between /11
0.5 and 0.67. In Fig.7, J_{ii} is plotted as a function of ℓ_P, shown as a broken line. The ion current exhibits a relatively sharp maximum at $\ell_P = 8.7$ mm. As also shown in Fig.7, the optimum extraction potential U_{eopt} increases with the

length of the bore in the plasma boundary armature ℓ_p. Two curves are plotted: one for a constant hole radius $r_p = 4.5$ mm and one for a fixed r_p/ℓ_p ratio of 0.5. The curves $J_{ii}(\ell_p)$ and $U_{e\,opt}(\ell_p)$ can be interpreted from the extraction ratios.

Finally, we also varied the cathode geometry. In Fig.8, the three efficiencies η_e, η_m, and η_{tot} are plotted as a function of the cathode channel radii r_K. The length of the 55 channel bores was $\ell_K = 3$ mm. The corresponding armature values were $\ell_p = 8.7$ mm, $r_p = 4.5$ mm. On increasing the channel apertures, in agreement with theory and experiment, there will be an increase in ion current J_{ii}, neutral gas stream J_O, focusing degree f_i, and electric efficiency η_e, while the ion loss current J_{iK} and the mass efficiency η_m will decrease. The total efficiency η_{tot} has a maximum at $r_K = 1$ mm.

The degree of focusing and other specific properties (at fixed r_p/ℓ_p and r_K/ℓ_K) depend on the quotient r_p/r_K. If this ratio is too large, f_i will decrease. The optimum value was found to be $r_p/r_K = 4.5$.

7. Summary

After its optimization, the test engine has the following geometry:

Discharge vessel: radius $r = 4.3$ cm, height $2R = 8.6$ cm, volume $V_v = 500\ cm^3$.

Plasma boundary armature: thickness $\ell_p = 8.7$ mm, 55 holes of radius $r_p = 4.5$ mm.

Cathode: thickness $\ell_K = 3$ mm, 55 holes of radius of 1 mm.

The tests showed the following optimum operating data: transmitter power $L_{tr} = 80$ w, transmitter frequency $f = 17.5$ mc, auxiliary magnetic field strength $H = 10$ oe, pressure $p = 10^{-4}$ torr, extraction potential $U_e = 5.5$ kv, afteracceleration potential 9.5 kv.

The following measured jet currents and powers were obtained: total ion current $J_i = 40$ ma, extracted useful ion current $J_{ii} = 39$ ma, ion loss current $J_{iK} = 1$ ma, neutral gas current $J_0 = 1.25 \times 10^{16}$/sec = 2 ma/$e_i$*, jet power L = = 585 w, cathode loss power 5.5 w, total loss power 85 w, electric efficiency $\eta_e = 87\%$, mass efficiency $\eta_m = 95\%$, total efficiency $\eta_{tot} = 83\%$.

BIBLIOGRAPHY

/12

1. Freisinger, J. and Löb, H.: WGLR Yearbook 1964, p.396.
2. Birkhoff, G.: Z. angew. Phys., Vol.10, p.204, 1958.
3. Reader, P.D.: NASA TM X-52042, 1964.
4. Neuert, H., Stuckenberg, H.J., and Weidner, H.P.: Z. angew. Phys., Vol.6, p.303, 1954.
5. Erö, J.: Nucl. Instr., Vol.3, p.303, 1958.
6. Löb, H.: Z. Naturforsch., Vol.16a, p.67, 1961.
7. Kamke, D. and Rose, H.J.: Z. Physik, Vol.145, p.83, 1956.
8. Reifenschweiler, O.: Ann. Phys. Lpz., Vol.14, p.33, 1954.

---

*J_0 is defined as (R = gas constant, A = atomic weight):

$$J_0 = Z \cdot \frac{r_K^2}{\frac{3}{8}\frac{l}{K} + 1} \cdot \sqrt{\frac{\pi R T_0}{2A}} \cdot n_0 \qquad (16)$$

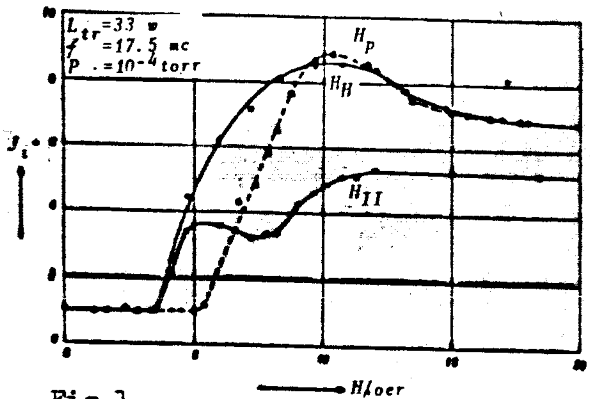

Fig.1

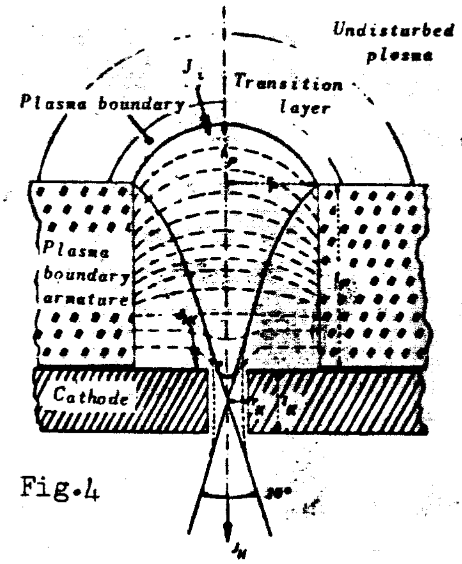

/13

Fig.4

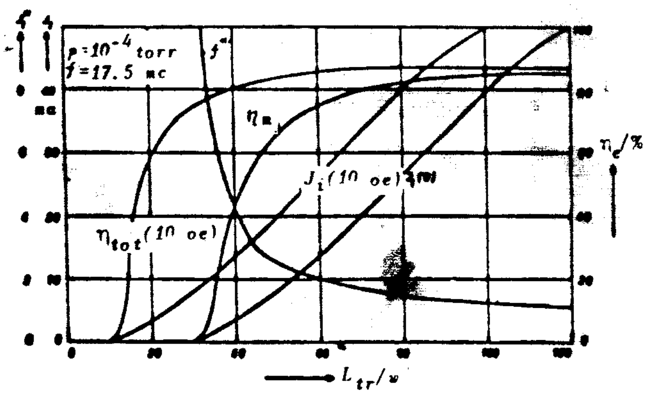

Fig.2

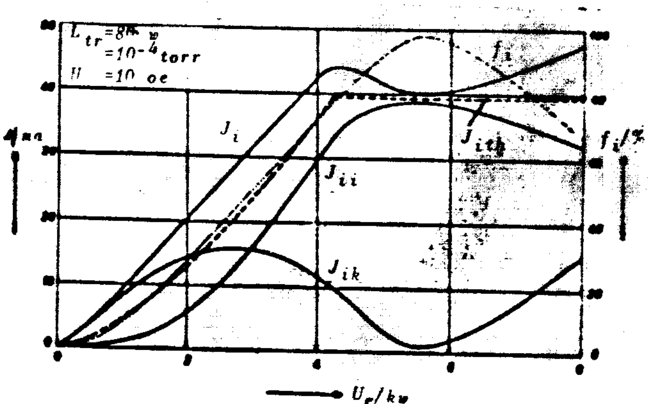

Fig.5

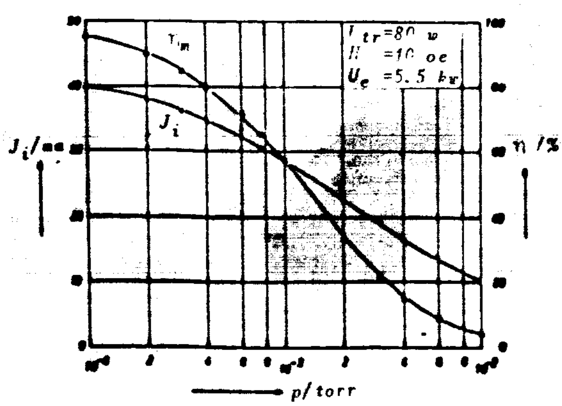

Fig.3

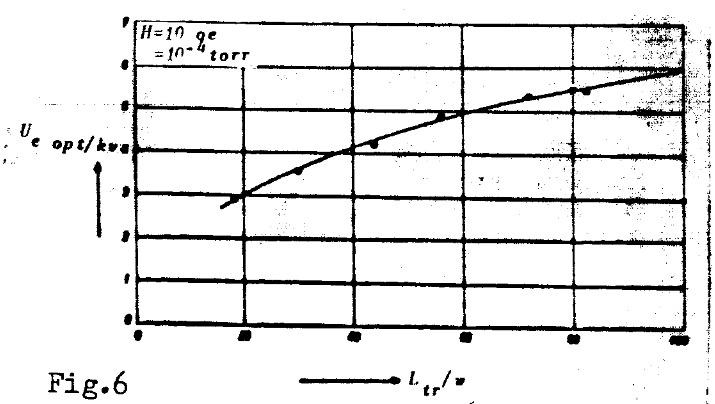

Fig.6

/13

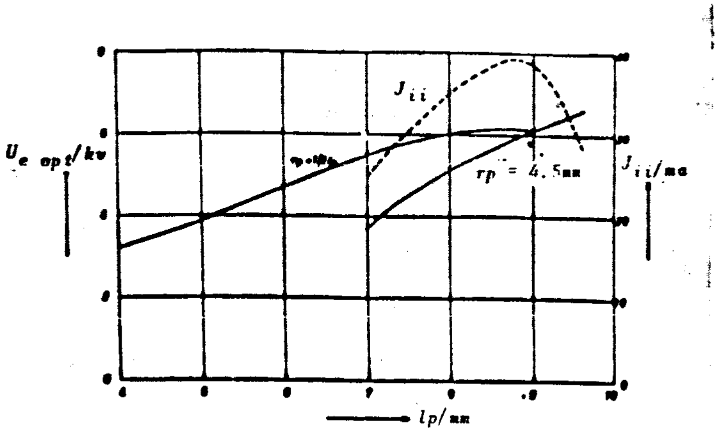
J_{ii}
U_e opt/kv
J_{ii}/ma
rp = 4.5mm
lp/mm

Fig.7

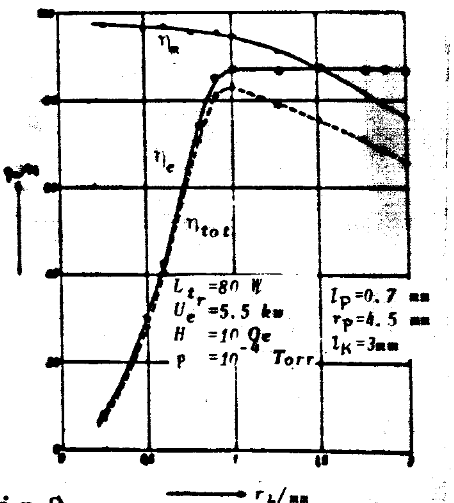
η_m
η_e
η_{tot}
L_{tr} =80 W
U_e =5.5 kv
H =10 Oe
p =10^{-4} Torr
l_p=0.7 mm
r_p=4.5 mm
l_K=3mm
r_k/mm

Fig.8

#375

TERMINOLOGY

Reference Works consulted include: Space Technology, by Seifert; Flight Performance Handbook, for Orbital Operation, by Wolverton; and others.

ion engine; tank circuit; waste heat; ion extraction; HF discharge; accelerator; eddy field; time of flight; Boltzmann; energy increment constant; capacitatively; self-sustaining; electrodeless; volume recombination; recombination event; ambipolar; Bessel function; extraction potential; Langmuir probe; Helmholtz coil; cyclotron effect; cathode channel transconductance; pinch; overfocused; underfocused; space-charge-limited; cathode sputtering; saturation current; Pierce geometry; Pierce oscillator; etc.